Spin and lattice excitations of a BiFeO3 thin film and ceramics

S Skiadopoulou, V Goian, C Kadlec, F Kadlec, Bai X.F., Ingrid C.Infante, B Dkhil, C Adamo, D.G. Schlom, S Kamba

HAL Id: hal-01258804
https://hal.science/hal-01258804

Submitted on 28 Aug 2020

Spin and lattice excitations of a BiFeO₃ thin film and ceramics

S. Skiadopoulou,[1, *] V. Goian,[1] C. Kadlec,[1] F. Kadlec,[1] X.F. Bai,[2]

I.C. Infante,[2] B. Dkhil,[2] C. Adamo,[3, 4] D.G. Schlom,[3, 5] and S. Kamba[1, †]

[1]*Institute of Physics, The Czech Academy of Sciences,*
Na Slovance 2, 182 21 Prague 8, Czech Republic
[2]*Laboratoire SPMS, UMR 8580, CentraleSupelec, CNRS,*
Université Paris-Saclay, Grande Voie des Vignes, Chatenay-Malabry, France
[3]*Department of Materials Science and Engineering,*
Cornell University, Ithaca, New York, 14853 USA
[4]*Department of Applied Physics, Stanford University, Stanford, CA 94305, USA*
[5]*Kavli Institute at Cornell for Nanoscale Science, Ithaca, New York, 14853 USA*
(Dated: August 27, 2018)

We present a comprehensive study of polar and magnetic excitations in BiFeO₃ ceramics and a thin film epitaxially grown on an orthorhombic (110) TbScO₃ substrate. Infrared reflectivity spectroscopy was performed at temperatures from 5 to 900 K for the ceramics and below room temperature for the thin film. All 13 polar phonons allowed by the factor-group analysis were observed in the ceramic samples. The thin-film spectra revealed 12 phonon modes only and an additional weak excitation, probably of spin origin. On heating towards the ferroelectric phase transition near 1100 K, some phonons soften, leading to an increase in the static permittivity.   In the ceramics, terahertz transmission spectra show five low-energy magnetic excitations including two which were not previously known to be infrared active; at 5 K, their frequencies are 53 and 56 cm⁻¹. Heating induces softening of all magnetic modes. At a temperature of 5 K, applying an external magnetic field of up to 7 T irreversibly alters the intensities of some of these modes. The frequencies of the observed spin excitations provide support for the recently developed complex model of magnetic interactions in BiFeO₃ (R.S. Fishman, Phys. Rev. B 87, 224419 (2013)). The simultaneous infrared and Raman activity of the spin excitations is consistent with their assignment to electromagnons.

I.   INTRODUCTION

Among novel materials, an intense effort is concentrated on the study of multiferroics.[1,2] A wide range of applications, such as information storage, sensing, actuation, and spintronics, await pioneering materials and strategies that would produce robust magnetoelectric coupling at room temperature (RT).[3,4] The ability to manipulate magnetization in a magnetoelectric multiferroic by electric fields can be extremely promising for such applications, due to the simplicity and cost-efficiency of applying an electric field. As one of the few single-phase RT magnetoelectric multiferroics, bismuth ferrite BiFeO₃, is at the center of attention, as it presents a ferroelectric phase transition at approximately 1100 K and an antiferromagnetic one at 643 K.[5]

The knowledge of lattice and spin excitations in BiFeO₃ is essential for understanding the underlying mechanisms that induce its multiferroic behavior. A series of Raman and Infrared (IR) spectroscopy studies have presented controversial results concerning the assignment of the magnon and phonon modes, as well as of the highly acclaimed electromagnons (i.e., electrically active magnons). Probing IR-active low-energy excitations is hindered by a lack of sufficiently large single crystals. Raman-active phonons of the rhombohedral $R3c$ BiFeO₃ structure have been reported for single crystals,[6-8] polycrystalline ceramics,[9-11] and thin films,[12,13] however,

there is a significant discrepancy between the claimed phonon frequencies and symmetry representations. A possible explanation for such inconsistences between the various experimental results is the presence of oblique phonon modes, which show a continuous variation of frequency along the phonon propagation vector with respect to the crystallographic axis of the probed specimen.[11] Up to now, the phonon IR spectroscopy studies have been focused on ceramics[14-16] and single crystals,[17,18] whereas, to our knowledge, no report of a thin-film IR investigation exists.

When it comes to magnon and electromagnon studies, Raman spectroscopy holds the record for the number of excitations observed, yielding up to 16 magnetic modes corresponding to the cycloidal spin structure (8 Φ_n cyclon and 8 Ψ_n extra-cyclon modes) for single crystals,[19-22] but only one for polycrystalline thin films.[23,24] Furthermore, the influence of strain on the number of spin excitations and their frequencies were reported for epitaxial thin films grown on a series of substrates.[25] Time-domain THz spectroscopy,[26] inelastic neutron scattering measurements[27-30] and absorbance spectroscopy in the THz range[31] have revealed modes similar to the Raman-active onespredicted by theoretical calculations.[31-35] The best agreement between the experimental and theoretical spin-excitation frequencies (including their splitting in external magnetic field) was obtained for a microscopic model that takes into ac-

count the nearest and next-nearest neighbor exchange interactions, two Dzyaloshinskii-Moriya interactions and an easy-axis anisotropy.[31,35] The same model successfully described the low-energy inelastic neutron scattering spectra.[30] In contrast, Komandin *et al.*[15] showed IR transmission spectra with an excitation at approximately $47 \, \text{cm}^{-1}$ which had not been previously reported by experimental or theoretical studies. The intensive discussion in the literature concerning the nature of the spin excitations raises the question: which excitations are pure magnons (i.e., contribute only to the magnetic permeability μ) and which are electromagnons (i.e., influence at least partially the permittivity ε^*)? It is worth noting that according to a recent symmetry analysis,[36] $BiFeO_3$ allows directional dichroism and therefore spin waves can be simultaneously excited by the electric and magnetic components of electromagnetic radiation. For more details on $BiFeO_3$ spin dynamics, see the review of Park *et al.*[37]

In the current work, we report spin and lattice excitations in $BiFeO_3$ ceramics, as measured by the combination of IR reflectivity and time-domain THz transmission spectroscopy, in a temperature range from 10 to $900 \, \text{K}$. All 13 IR-active phonon modes are observed, exhibiting softening on heating. Five low-frequency spin modes are detected from $5 \, \text{K}$ up to RT, the highest two appearing at 53 and $56 \, \text{cm}^{-1}$. This corresponds to the frequency range where such excitations were theoretically predicted,[31,32,35] but not experimentally confirmed up to now. At $5 \, \text{K}$, the low-energy spin dynamics in the THz range were also studied in a varying magnetic field of up to $7 \, \text{T}$. Softening of the (electro)magnon frequencies upon increasing the magnetic field was observed. Additionally, a $BiFeO_3$ epitaxial thin film grown on an orthorhombic (110) $TbScO_3$ single crystal substrate was studied for the first time via IR reflectance spectroscopy.

II. EXPERIMENTAL DETAILS

$BiFeO_3$ ceramics were prepared by the solid-state route. A stoichiometric mixture of Fe_2O_3 and Bi_2O_3 powder oxides with a purity of 99.99% was ground and uniaxially cold-pressed under 20-30 MPa pressure into 8 mm diameter pellets. The pellets were then covered by sacrificial BFO powder to avoid bismuth oxide loss from the pellet, and sintered in a tube furnace at $825 \, °\text{C}$ for 8 h in air. To avoid any secondary phase formation, the samples were quenched to RT. Polished disks with a diameter of 4 mm and thicknesses of ca. 600 and $338 \, \mu\text{m}$ were used for the IR reflectivity and THz transmission measurements, respectively.

An epitaxial $BiFeO_3$ thin film with a thickness of 300 nm was grown by reactive molecular-beam epitaxy on a (110) single crystal substrate. The growth parameters were the same as for the samples reported in Ref. [38]. Near-normal incidence IR reflectivity spectra of the $BiFeO_3$ ceramics and film were obtained using

a Fourier-transform IR spectrometer Bruker IFS 113v in the frequency range 20–$3000 \, \text{cm}^{-1}$ (0.6–90 THz) at RT; for the low and high temperature measurements the spectral range was reduced to $650 \, \text{cm}^{-1}$. Pyroelectric deuterated triglycine sulfate detectors were used for the room- and high-temperature measurements up to 900 K, whereas a He-cooled (operating temperature 1.6 K) Si bolometer was used for the low-temperature measurements down to 10 K. A commercial high-temperature cell (SPECAC P/N 5850) was used for the high-temperature experiments. The thermal radiation from the hot sample entering the interferometer was taken into account in our spectra evaluation.

THz measurements from $3 \, \text{cm}^{-1}$ to $60 \, \text{cm}^{-1}$ (0.09–1.8 THz) were performed in the transmission mode with the use of a custom-made time-domain terahertz spectrometer. In this spectrometer, a femtosecond Ti:sapphire laser oscillator (Coherent, Mira) produces a train of femtosecond pulses which generates linearly polarized broadband THz pulses in a photoconducting switch TeraSED (Giga-Optics). A gated detection scheme based on electrooptic sampling with a 1 mm thick [110] ZnTe crystal as a sensor allows us to measure the time profile of the electric field of the transmitted THz pulse. The same high-temperature cell as for the IR reflectivity was used for the THz range high-temperature measurements. Oxford Instruments Optistat optical cryostats with mylar and polyethylene windows were used for the low-temperature THz and IR measurements, respectively. THz experiments in an external magnetic field $H_{\text{ext}} \leq 7 \, \text{T}$ were performed upon decreasing H with an Oxford Instruments Spectromag cryostat in the Voigt configuration, where the electric component of the THz radiation $\mathbf{E}_{\text{THz}}$ was set perpendicular to H_{ext}.

The IR reflectivity and THz complex (relative) permittivity spectra $\varepsilon^*(\omega)$ were carefully fit assuming the factorized form of the dielectric function based on a generalized damped-harmonic-oscillator model:[39]

$$\varepsilon^*(\omega) = \varepsilon_\infty \prod_{j=1}^{N} \frac{\omega_{\text{LOj}}^2 - \omega^2 + i\omega\gamma_{\text{LOj}}}{\omega_{\text{TOj}}^2 - \omega^2 + i\omega\gamma_{\text{TOj}}}, \tag{1}$$

where ω_{TOj} and ω_{LOj} are the frequencies of the j-th transverse optical (TO) and longitudinal optical (LO) phonons, γ_{TOj} and γ_{LOj} are the corresponding damping constants, and ε_∞ denotes the high-frequency (electronic) contribution to the permittivity, determined from the RT frequency-independent reflectivity tail above the phonon frequencies. The reflectivity $R(\omega)$ is related to the complex dielectric function $\varepsilon^*(\omega)$ by:

$$R(\omega) = \left| \frac{\sqrt{\varepsilon^*(\omega)} - 1}{\sqrt{\varepsilon^*(\omega)} + 1} \right|. \tag{2}$$

To evaluate the IR reflectance spectra of the $BiFeO_3/TbScO_3$ thin film, a model corresponding to a two-layer optical system was used.[40] The IR reflectivity spectra of the bare $TbScO_3$ substrate were fit first at each
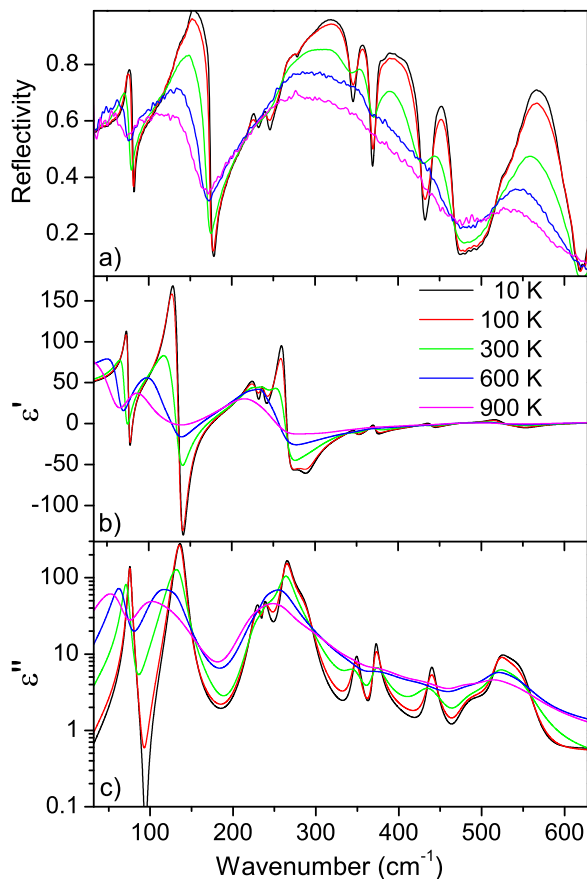
FIG. 1: (Color online) (a) IR reflectivity spectra of BiFeO$_3$ ceramics at selected temperatures; (b) Real, and (c) imaginary part of permittivity, as obtained from the fits.

temperature, using the model described by Eq. 1. The values of oscillator parameters ($\omega_{\text{TO}j}$, $\omega_{\text{LO}j}$, $\gamma_{\text{TO}j}$, $\gamma_{\text{LO}j}$, and ε_∞) obtained for the substrate were used for fitting the BiFeO$_3$/TbScO$_3$ thin-film spectra. The model used to describe the complex permittivity of the thin film is a sum of N independent three-parameter damped harmonic oscillators, which can be expressed as:[39]

$$\varepsilon^*(\omega) = \varepsilon_\infty + \sum_{j=1}^{N} \frac{\Delta\varepsilon_j \omega_{\text{TO}j}^2}{\omega_{\text{TO}j}^2 - \omega^2 + i\omega\gamma_{\text{TO}j}}, \qquad (3)$$

where $\Delta\varepsilon_j$ is the dielectric strength of the j-th mode. Eq. 3 is simpler than Eq. 1, and its use is well justified because the damping of the LO phonons of the film does not appreciably influence the reflectance spectra.

III. RESULTS AND DISCUSSION

A. Phonons in the BiFeO$_3$ ceramics

The temperature dependence of the experimental IR reflectivity spectra of the BiFeO$_3$ ceramics is shown in Fig. 1(a). The reflectivity band intensities are higher than those in the previously published spectra of ceramics[14–16] and single crystal,[18] but comparable to the single-crystal spectra published by Lobo et al.[17] This confirms the very high quality and density of our ceramic samples, which is essential for an accurate determination of phonon and magnon parameters.

The IR reflectivity and THz transmission spectra were fit simultaneously using Eq. 1; the resulting phonon parameters are listed in Table 1. The real and imaginary parts of the complex dielectric spectra calculated from the fits are shown in Figs. 1(b),(c). As predicted by the factor group analysis for the rhombohedral $R3c$ structure of BiFeO$_3$,[14] all 13 IR-active phonons ($4A_1 + 9E$ symmetries) are clearly seen from 10 K up to RT. In Table 1, the symmetries of all modes are assigned based on Raman spectra,[11] first-principles calculations,[41] and IR spectra of single crystals.[17] The damping of the modes strongly increases on heating; therefore, above 300 K, the IR reflection bands broaden and mutually overlap. Note the remarkable softening of the modes below 150 cm^{-1} upon heating (see Fig. 1). Consequently, the static permittivity $\varepsilon(0)$ determined by the sum of phonon contributions as $\varepsilon(0) = \varepsilon_\infty + \sum \Delta\varepsilon_j$ increases on heating in agreement with the Lyddane-Sachs-Teller relation[42] (see Fig. 2). A qualitatively similar temperature dependence was published in previous studies of BiFeO$_3$ ceramics,[14,15] but the absolute value of permittivity was lower, probably due to a lower density/quality of the earlier studied ceramics. In contrast, the permittivity calculated from the single-crystal spectra[17] is slightly higher, due to the absence of the A_1 modes whose dielectric strength $\Delta\varepsilon_j$ is lower than the E-symmetry modes.

We would like to stress that the temperature dependence of permittivity calculated from the phonon contributions has been previously published mostly below RT,[15,17] and only Ref. 14 reported $\varepsilon(0,T)$ up to 900 K. Experimental low-frequency (i.e., below 1 MHz) dielectric data are also not available above RT due to the presence of significant leakage currents in BiFeO$_3$ at high temperatures. There is only one publication[16] presenting IR spectra of BiFeO$_3$ ceramics up to 1280 K, i.e., far above T_C, however, in this case, emissivity was measured instead of reflectivity above 600 K and $\varepsilon(0,T)$ was not reported. In that work, Massa et al.[16] listed phonon parameters at selected temperatures, from which we recalculated $\varepsilon(0,T)$; these values are presented for sake of comparison in Fig. 2. One can see that, at $T = 523$ and 850 K, Massa et al.[16] obtained the lowest published values of $\varepsilon(0)$. We also note the unusual increase in ε_∞ and $\varepsilon(0,T)$ on cooling below RT; the latter appears to be in contradiction with the soft-mode frequency increase on cooling, reported in the same work. Finally, two additional phonon modes at $T = 4$ K, not predicted by the factor-group analysis, are reported in Ref. 16. All these facts raise questions about whether these results describe the intrinsic properties of BiFeO$_3$. Nevertheless, it is worth noting the peak in Massa's data at the ferroelec-

TABLE I: A comparison of the parameters of the IR-active modes in the BiFeO$_3$ ceramics (at 10 and 900 K) and the thin film (at 10 K), obtained from IR spectra fitting. The symmetry assignment of each mode is also given.

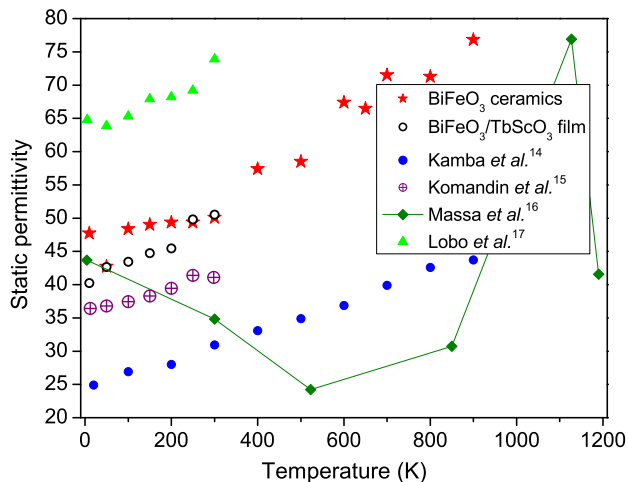| | Ceramics | | | | | | | | Thin film | | | | | |
| | 10 K | | | | 900 K | | | | 10 K ($\mathbf{E}_{\text{ext}} \parallel [1\bar{1}0]$) | | | 10 K ($\mathbf{E}_{\text{ext}} \parallel [001]$) | | |
Symmetry	ω_{TO}	γ_{TO}	ω_{LO}	γ_{LO}	ω_{TO}	γ_{TO}	ω_{LO}	γ_{LO}	ω_{TO}	γ_{TO}	$\Delta\varepsilon$	ω_{TO}	γ_{TO}	$\Delta\varepsilon$
E	75.8	4.6	81.5	2.8	64.3	40.9	70.5	19.3	74.7	1.4	4.3	77.8	1.8	4.5
E	133.7	22.8	137.4	34.6	101.0	65.1	117.9	51.1	132.2	2.3	8.6	136.7	2.9	12.2
A_1	137.8	13.6	175.8	4.0	124.3	57.6	165.8	32.9	145.2	2.4	7.4			
A_1	231.2	14.0	233.9	5.6	226.2	59.6	233.5	31.4	225.9	2.9	0.6	227.4	2.2	0.7
E	236.7	7.6	243.6	13.3	234.0	31.7	240.8	69.3	241.0	4.3	0.9	242.4	4	0.2
E	264.0	13.0	283.0	38.0	258.2	60.4	278.0	48.5	266.2	2.3	5.4	266.8	4.4	0.4
E	288.5	26.2	345.8	9.2	278.4	61.6	340.7	40.4	293.9	4.6	3.6	279.5	5.5	10.6
E	349.0	10.0	368.1	5.0	342.5	42.5	363.6	41.0						
E	372.0	7.3	430.7	10.6	364.5	50.1	420.3	51.4				371.7	9.2	0.9
E	439.6	11.0	468.0	13.3	424.0	54.3	464.3	37.1				445.7	0.3	1.1
A_1	476.2	41.2	503.7	49.1	469.8	41.0	502.8	106.2	472.2	7.1	0.01			
E	520.2	21.8	523.8	76.0	514.7	45.7	518.3	62.5	524.0	9.8	0.3	516.8	12.7	0.04
A_1	549.5	36.9	606.2	27.1	542.1	78.8	595.3	102.3	550.6	7.2	0.07	551.8	2.3	1
spin wave												603.6	9.9	0.01

FIG. 2: (Color online) Temperature dependence of the static permittivity calculated from the sum of phonon contributions. The data for the ceramics and the film ($\mathbf{E}_{\text{ext}} \parallel [1\bar{1}0]$) from the current work are compared with previously published data obtained, in order, on ceramics,[14–16] and a single crystal.[17] The line connecting the data from Ref. [16] is a guide for the eyes. See the text for additional details.

tric phase transition near 1120 K; this is the only experiment showing a dielectric anomaly at T_C in BiFeO$_3$. The peak is much lower than in other canonical ferroelectrics, apparently due to the first-order character of the phase transition from $R3c$ symmetry to the high-temperature $Pnma$ structure.[5,37]

B. Excitations in the BiFeO$_3$ thin film

The polarized IR reflectivity spectra of the bare (110) TbScO$_3$ substrate and reflectance spectra of the BiFeO$_3$/TbScO$_3$ thin film are shown in Fig. 3. All BiFeO$_3$ mode frequencies obtained by fitting are listed in Table 1. We note that, on the one hand, the BiFeO$_3$ phonons below 150 cm^{-1} are better resolved in the $\mathbf{E}_{\text{ext}} \parallel [1\bar{1}0]$ polarization with respect to the substrate crystal axes, because the TbScO$_3$ phonons are weak in this case. On the other hand, the BiFeO$_3$ modes at 372 and 446 cm^{-1} are seen only in the $\mathbf{E}_{\text{ext}} \parallel [001]$ polarized spectra, due to a more favorable TbScO$_3$ spectrum in this region. Namely, the large TO-LO splitting of the TbScO$_3$ phonons within 370–480 cm^{-1} enhances the sensitivity of the IR reflectance to the thin-film phonons.[43] Therefore, due to the properties of TbScO$_3$, the two polarizations provide complementary information on the BiFeO$_3$ response. Note that some TbScO$_3$ phonons seen below 150 cm^{-1} (see Fig. 3) exhibit anomalous temperature shifts and even splitting on cooling. This is probably caused by phonon interaction with the crystal field (and related electronic transitions).[44]

The in-plane lattice parameters of the (110) TbScO$_3$ substrate are slightly smaller than those of BiFeO$_3$, inducing only a small compressive strain ($\sim 0.24\%$) in the $(001)_{\text{cub}}$ epitaxial film. Here, the orientation of the thin film is marked with respect to the pseudocubic crystal axis (which is denoted by the subscript "cub") of BiFeO$_3$. The ferroelastic and ferroelectric domain structure of BiFeO$_3$/TbScO$_3$ was investigated in Refs. [38,45] where two kinds of stripe-like domains separated by $(010)_{\text{cub}}$ vertical boundaries were reported. The spontaneous po-
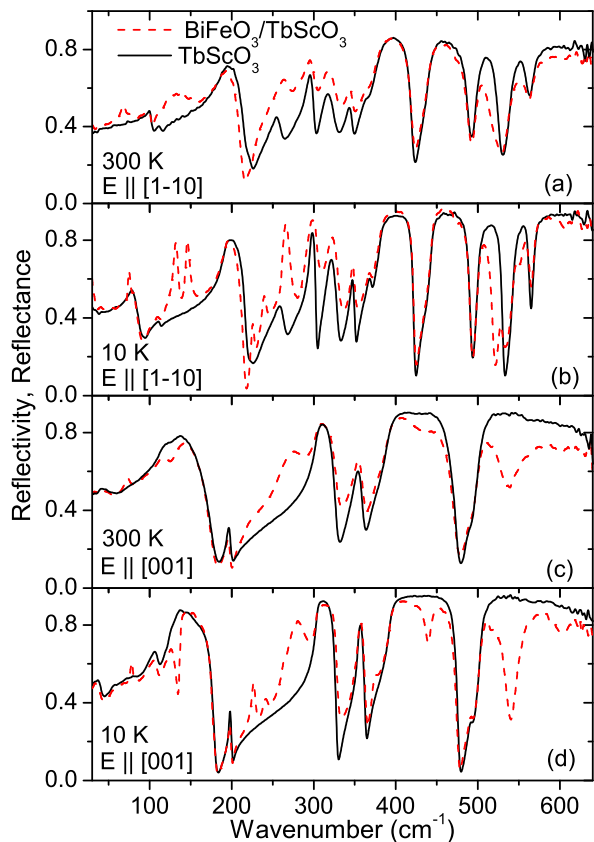
FIG. 3: (Color online) Room-temperature and 10 K IR reflectivity spectra of the TbScO$_3$ substrate and reflectance of the BiFeO$_3$/TbScO$_3$ thin film for polarizations (a,b) $\mathbf{E}_{ext} \parallel [1\bar{1}0]$ and (c,d) $\mathbf{E}_{ext} \parallel [001]$.

larization $\mathbf{P}$ in adjacent domains is rotated by 109° and its direction is tilted from the $[001]_{cub}$ direction.[45] In our IR spectra, only vibrations polarized in the film plane are active. Since the ferroelectric polarization $\mathbf{P}$ is tilted from the normal of the thin film plane, phonons of both E and A_1 symmetries can be excited. Nevertheless, we see only some of the modes due to our limited sensitivity to the thin film. In contrast to the ceramics samples, the phonon damping observed in the thin film is much lower (see Table 1). The values of the damping constants are comparable to those of single crystals,[17] which confirms the high quality of our epitaxial thin film. Similar to the case of BiFeO$_3$ ceramics, the phonon eigenfrequencies in the film decrease on heating, leading to an increase in the static permittivity $\varepsilon(0, T)$ (see Fig. 2). The phonon frequencies of the BiFeO$_3$ ceramics and the film present no significant differences, which is clearly a consequence of the very small strain applied to the film by the substrate. The calculated $\varepsilon(0, T)$ is, however, smaller in the BiFeO$_3$ film than in the single crystal (see Fig. 2), because, for the former sample, only strong phonons were revealed in the IR reflectance spectra.

In the low-temperature $\mathbf{E}_{ext} \parallel [001]$ spectra, a weak

but sharp and clearly observable minimum in reflectance develops near 600 cm^{-1} (see Fig. 3(d)). We can exclude its phonon origin, because the factor-group analysis in rhombohedral structure does not allow an additional mode. A lower crystal symmetry is also excluded because our thin film has only 0.24% compressive strain; it is known that the films change the structure only with strain higher than 2%.[46] Also the multi-phonon origin is not likely since multi-phonon scattering usually decays on cooling; at RT, the peak intensity is markedly lower, close to our sensitivity limit (see Fig. 3(c)). Interestingly, the position of the peak, ca. 604 cm^{-1}, corresponds to the maximum magnon energy observed out of the Brillouin-zone center by inelastic neutron scattering in a BiFeO$_3$ single crystal.[27] Therefore, we assign this peak to scattering by the highest-energy part of the magnon branch. The magnon density of states can be activated in the IR spectra due to the modulated cycloidal magnetic structure of BiFeO$_3$; the maxima in the density of states occur either at the maximal energy or at the Brillouin-zone boundary. Correspondingly, another peak in the density of states can be expected for the magnon branch at the K and M points. These magnons have an energy[30] of ca. 525 cm^{-1}, which falls into the range of the highest-energy phonon. We assume that this strong phonon screens the weak magnon signal, which is why we do not detect the corresponding absorption in the IR spectra. Finally, let us mention that the magnons from the Brillouin-zone boundary become frequently electrically active due to the exchange striction;[47] therefore, they can be called electromagnons.

C. Magnetic excitations in THz spectra of BiFeO$_3$ ceramics

Our efforts to measure THz spectra of the BiFeO$_3$ film failed, due to insufficient signal. This can be explained by the fact that the thin film only slightly absorbs the THz pulses and the index of refraction n of BiFeO$_3$ is higher than that of the substrate only by $\approx 50\%$. We note that time-domain THz spectroscopy can be used only for studies of the thin films with n at least one order of magnitude higher than that of the substrate. As an example, such a technique was successfully used for investigation of the ferroelectric soft mode behavior near a strain-induced ferroelectric phase transition in SrTiO$_3$ thin films.[48]

In contrast, THz spectra of the BiFeO$_3$ ceramics were successfully measured at temperatures from 5 to 900 K. The spectra of the complex refractive index $N(\omega) = n(\omega) + ik(\omega)$, determined from experimental data for various temperatures, are presented in Fig. 4. In magnetic systems, N depends on the complex permittivity ε^* and permeability μ^* via the relationship $N(\omega) = \sqrt{\mu^* \varepsilon^*}$. Since we cannot resolve whether the observed modes contribute to μ^* (as magnons) or ε^* (as electromagnons or polar phonons), we only present $n(\omega)$, $k(\omega)$ spectra in
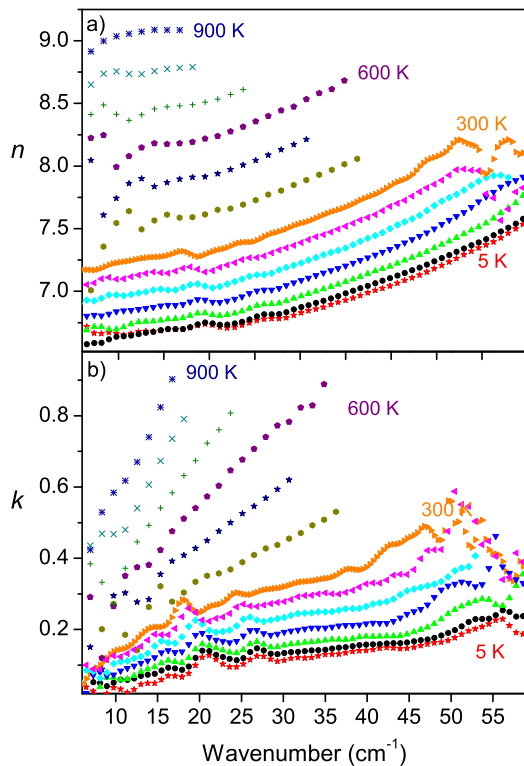
FIG. 4: (Color online) Temperature dependences of the (a) refractive index and (b) extinction coefficient spectra of $BiFeO_3$ ceramics, determined from the THz transmission. The spectra are shown for every 50 and 100 K below and above RT, respectively.

Fig. 4.

In the THz spectra, one can see a gradual increase in n and k on heating. This is mainly caused by the softening of the TO_1 phonon and an increase in the phonon damping with heating. The weak maxima in the $k(\omega)$ spectra correspond to frequencies of magnetic excitations. Their temperature dependence is plotted in Fig. 5 together with the modes observed in Raman[20,21] and IR[26,31] spectra. Note that the modes between 32 and 44 cm^{-1} become IR–active only in external magnetic field.[31,35] Besides a good agreement between the frequencies of Raman and IR–active modes, one can see a gradual decrease in all mode frequencies with increasing temperature. Although the excitations should exist at least up to T_N, we fit our THz spectra only up to 300 K, because, above RT, their damping is very high, precluding their exact fitting. We clearly distinguish five magnetic excitations. The three of them appearing up to 27 cm^{-1} correspond to the IR-active modes observed earlier by other authors.[15,26,31] In our spectra, they exhibit an enhanced damping in comparison with single-crystal data, mainly due to the fact that we measured un-polarized spectra. At 5 K, two modes are seen with peak absorption frequencies of 53 cm^{-1} and 56 cm^{-1}. These modes were not observed in IR spectra before, apparently because the samples used in
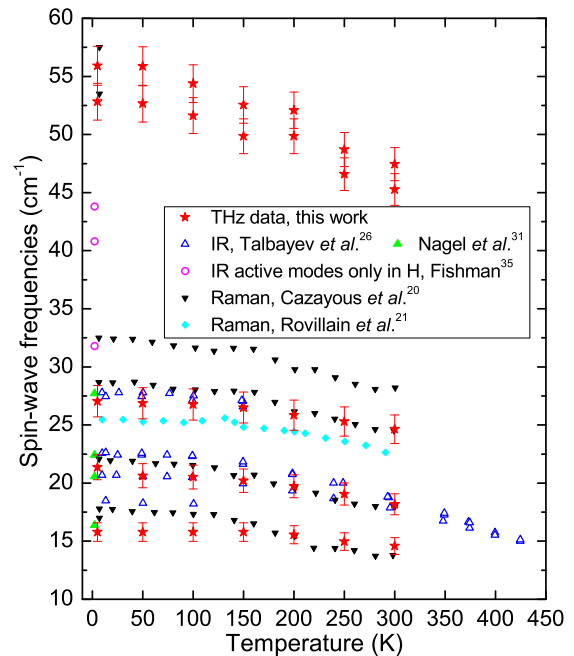

FIG. 5: (Color online) Temperature dependence of the spin-excitation frequencies determined by fits of the absorption index spectra in the THz range compared with published frequencies obtained from Raman scattering[20,21] and far IR spectra[31]. The modes at $\sim$ 32, 41 and 44 cm^{-1} were predicted by Fishman[35] and they become IR–active only in magnetic field above 7 T.[31]
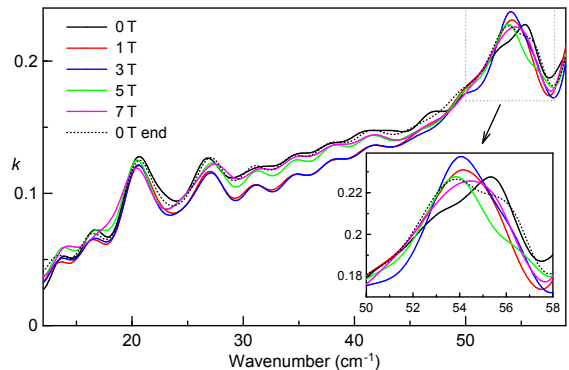

FIG. 6: (Color online) Magnetic field dependence of the experimental THz extinction coefficient in the $BiFeO_3$ ceramics measured at 5 K. The dotted line shows the zero-field spectrum after applying the magnetic field.

previous studies were opaque above 40 cm^{-1}. These peak frequencies correspond well to the Ψ_7 and Φ_8 modes reported in Raman spectra by Cazayous et al.[20] Note that Komandin et al.[15] predicted a polar and heavily damped mode at an estimated frequency of 47 cm^{-1}, but their rough estimation was based on discrepancies between IR reflectivity and THz transmission spectra. Nagel et al.[31] discovered additional spin excitations near 40 and

$43\,\mathrm{cm}^{-1}$, but a magnetic field higher than $5\,\mathrm{T}$ was needed for the activation of these excitations in far-IR transmission spectra. Furthermore, Fishman predicted[35] a mode above $50\,\mathrm{cm}^{-1}$, which should soften in an external magnetic field, and de Sousa *et al.* predicted[32] exactly the two modes which we observe.

We measured THz transmittance at $5\,\mathrm{K}$ under a magnetic field up to $7\,\mathrm{T}$ (see the $k(\omega)$ spectra in Fig. 6). All modes exhibit small frequency shifts with increasing magnetic field. A similar behavior was reported by Nagel *et al.*,[31] but their frequency shifts were higher due to much higher values of the applied magnetic field (up to $31\,\mathrm{T}$). We see also weak indications of the modes near 32, 35, 38, and $42\,\mathrm{cm}^{-1}$, which correspond well (except the one at $35\,\mathrm{cm}^{-1}$) to the magnetic-field induced modes of Ref. [31]. In our measurements, while the sample was kept at a temperature of $5\,\mathrm{K}$, applying the magnetic field of $7\,\mathrm{T}$ irreversibly changed the shape of the magnetic modes in the absorption index spectrum (see Fig. 6), similarly to the observations in Ref. [31]. This behavior is probably a consequence of magnetic-field-induced changes in the geometry of magnetic domains and pinning the domain walls on defects. The pronounced modes near 53 and $56\,\mathrm{cm}^{-1}$ can be identified with the pair of modes predicted by Fishman near $45\,\mathrm{cm}^{-1}$ at $H_{\mathrm{ext}} = 15\,\mathrm{T}$.[35] Thus, our observations confirm the complex effective Hamiltonian describing the magnetic interactions in $BiFeO_3$; it includes nearest and next-nearest-neighbor exchange interactions, two Dzyaloshinskii-Moriya interactions, and an easy-axis anisotropy.[35] Very recently, this model was also confirmed by low-energy inelastic neutron scattering spectra.[30]

We were not able to fit unambiguously the THz spectra above $300\,\mathrm{K}$ using the modes seen at low temperatures, owing to their heavy damping at high temperatures. Nevertheless, a fit with one effective overdamped mode provided reasonable results. Surprisingly, this overdamped mode with a relaxation frequency around $15\,\mathrm{cm}^{-1}$ and $\Delta\varepsilon = 0.5$–1.2 ($\Delta\varepsilon$ rising with T) was necessary even above T_{N}, suggesting that there are still some paramagnons present in the paramagnetic phase. Alternatively, this mode might be due to a multiphonon or quasi-Debye absorption allowed in the noncentrosymmetric phase.[49]

Finally, we would like to stress that from unpolarized THz spectra, we could not distinguish whether our magnetic excitations are magnons or electromagnons. The symmetry analysis published by Szaller *et al.*,[36] however, allows electromagnons in the cycloidal G-type antiferromagnetic phase of $BiFeO_3$. In analogy with selection rules for polar phonons which, in acentric lattices, are both IR and Raman active, we suggest that for spin excitations, their simultaneous IR and Raman activites indicate that they are electromagnons. During the review process, the polar activity of spin excitations has been confirmed by Kézsmárki *et al.*,[50] who observed directional dichroism[36,51] of a $BiFeO_3$ single crystal in polarized far-IR spectra between 10 and $30\,\mathrm{cm}^{-1}$.

IV. CONCLUSIONS

An extensive study of IR vibrational spectra of $BiFeO_3$ ceramics and an epitaxial thin film is reported. The intensities of all phonons observed in the ceramics are higher than in the previous publications.[14–16] Thus, the static permittivity of our samples calculated from phonon contributions is close to the previously published single crystal data.[17] Some phonons slightly soften on heating, leading to an increase in the permittivity towards T_{C}. Nevertheless, the permittivity is much lower than in canonical ferroelectric perovskites, such as $BaTiO_3$ and $KNbO_3$, because the phonons in $BiFeO_3$ are much harder and the Born effective charges are much smaller. In addition, the phonons in a $BiFeO_3/TbScO_3$ epitaxial thin film were studied for the first time, showing parameters similar to those in $BiFeO_3$ single crystals. In the thin film, an additional weak excitation near $600\,\mathrm{cm}^{-1}$ was detected which apparently corresponds to a peak in the magnon density of states and which can be excited due to the incommensurately modulated magnetic structure of $BiFeO_3$. Time-domain THz spectra of $BiFeO_3$ ceramics reveal most of the spin excitations previously observed in single crystals.[26,31] Also, at $5\,\mathrm{K}$, a pair of IR-active modes near $55\,\mathrm{cm}^{-1}$ were observed, which corresponds to spin excitations theoretically predicted by de Sousa *et al.*[32] and Fishman.[35] This observation confirms the particular form of the Hamiltonian suggested by Fishman for the explanation of the magnetic interactions in $BiFeO_3$.

* Electronic address: stella@fzu.cz
† Electronic address: kamba@fzu.cz
[1] M. Fiebig, J. Phys. D: Appl. Phys. **38**, R123 (2005).
[2] Y. Tokura, S. Seki, and N. Nagaosa, Rep. Prog. Phys. **77**, 076501 (2014).
[3] W. Eerenstein, N. D. Mathur, and J. F. Scott, Nature **442**,

759 (2006).

[4] N. A. Spaldin, S. W. Cheong, and R. Ramesh, Physics Today **63**, 38 (2010).

[5] G. Catalan and J. F. Scott, Adv. Mater. **21**, 2463 (2009).

[6] R. Haumont, J. Kreisel, P. Bouvier, and F. Hippert, Phys. Rev. B **73**, 132101 (2006).

[7] H. Fukumura, S. Matsui, H. Harima, T. Takahashi, T. Itoh, K. Kisoda, M. Tamada, Y. Noguchi, and M. Miyayama, J. Phys.: Condens. Matter **19**, 365224 (2007).

[8] R. Palai, H. Schmid, J. F. Scott, and R. S. Katiyar, Phys. Rev. B **81**, 064110 (2010).

[9] D. Kothari, V. R. Reddy, V. G. Sathe, A. Gupta, A. Banerjee, and A. M. Awasthi, J. Magn. Magn. Mater. **320**, 548 (2008).

[10] D. Rout, K.-S. Moon, and S.-J. L. Kang, J. Raman Spectroscopy **40** (2009).

[11] J. Hlinka, J. Pokorný, S. Karimi, and I. M. Reaney, Phys. Rev. B **83**, 020101 (2011).

[12] M. K. Singh, H. M. Jang, S. Ryu, and M.-H. Jo, Appl. Phys. Lett. **88**, 042907 (2006).

[13] R. Palai, J. F. Scott, and R. S. Katiyar, Phys. Rev. B **81**, 024115 (2010).

[14] S. Kamba, D. Nuzhnyy, M. Savinov, J. Šebek, J. Petzelt, J. Prokleška, R. Haumont, and J. Kreisel, Phys. Rev. B **75**, 024403 (2007).

[15] G. Komandin, V. Torgashev, A. Volkov, O. Porodinkov, I. Spektor, and A. Bush, Phys. Sol. State **52** (2010).

[16] N. E. Massa, L. del Campo, D. de Souza Meneses, P. Echegut, G. F. L. Fabbris, G. d. M. Azevedo, M. J. Martnez-Lope, and J. A. Alonso, J. Appl. Phys. **108**, 084114 (2010).

[17] R. P. S. M. Lobo, R. L. Moreira, D. Lebeugle, and D. Colson, Phys. Rev. B **76**, 172105 (2007).

[18] J. Lu, M. Schmidt, P. Lunkenheimer, A. Pimenov, A. A. Mukhin, V. D. Travkin, and A. Loidl, J. Phys.: Conf. Series **200**, 012106 (2010).

[19] M. K. Singh, R. S. Katiyar, and J. F. Scott, J. Phys.: Condens. Matter **20**, 252203 (2008).

[20] M. Cazayous, Y. Gallais, A. Sacuto, R. de Sousa, D. Lebeugle, and D. Colson, Phys. Rev. Lett. **101**, 037601 (2008).

[21] P. Rovillain, M. Cazayous, Y. Gallais, A. Sacuto, R. P. S. M. Lobo, D. Lebeugle, and D. Colson, Phys. Rev. B **79**, 180411 (2009).

[22] P. Rovillain, R. de Sousa, Y. Gallais, A. Sacuto, M. A. Masson, D. Colson, A. Forget, M. Bibes, A. Barthélémy, and M. Cazayous, Nature Mater. **9**, 975 (2010).

[23] A. Kumar, J. F. Scott, and R. S. Katiyar, Appl. Phys. Lett. **99**, 062504 (2011).

[24] A. Kumar, J. F. Scott, and R. S. Katiyar, Phys. Rev. B **85**, 224410 (2012).

[25] D. Sando, A. Agbelele, D. Rahmedov, J. Liu, P. Rovillain, C. Toulouse, I. C. Infante, A. P. Pyatakov, S. Fusil, E. Jacquet, et al., Nature Mater. **12**, 641 (2013).

[26] D. Talbayev, S. A. Trugman, S. Lee, H. T. Yi, S.-W. Cheong, and A. J. Taylor, Phys. Rev. B **83**, 094403 (2011).

[27] J. Jeong, E. A. Goremychkin, T. Guidi, K. Nakajima, G. S. Jeon, S.-A. Kim, S. Furukawa, Y. B. Kim, S. Lee, V. Kiryukhin, et al., Phys. Rev. Lett. **108**, 077202 (2012).

[28] O. Delaire, M. B. Stone, J. Ma, A. Huq, D. Gout, C. Brown, K. F. Wang, and Z. F. Ren, Phys. Rev. B **85**, 064405 (2012).

[29] Z. Xu, J. Wen, T. Berlijn, P. M. Gehring, C. Stock, M. B. Stone, W. Ku, G. Gu, S. M. Shapiro, R. J. Birgeneau, et al., Phys. Rev. B **86**, 174419 (2012).

[30] J. Jeong, M. D. Le, P. Bourges, S. Petit, S. Furukawa, S.-A. Kim, S. Lee, S. Cheong, and J.-G. Park, Phys. Rev. Lett. **113**, 107202 (2014).

[31] U. Nagel, R. S. Fishman, T. Katuwal, H. Engelkamp, D. Talbayev, H. T. Yi, S.-W. Cheong, and T. Rõõm, Phys. Rev. Lett. **110**, 257201 (2013).

[32] R. de Sousa and J. E. Moore, Phys. Rev. B **77**, 012406 (2008).

[33] R. S. Fishman, N. Furukawa, J. T. Haraldsen, M. Matsuda, and S. Miyahara, Phys. Rev. B **86**, 220402 (2012).

[34] R. S. Fishman, J. T. Haraldsen, N. Furukawa, and S. Miyahara, Phys. Rev. B **87**, 134416 (2013).

[35] R. S. Fishman, Phys. Rev. B **87**, 224419 (2013).

[36] D. Szaller, S. Bordács, V. Kocsis, T. Rõõm, U. Nagel, and I. Kézsmárki, Phys. Rev. B **89**, 184419 (2014).

[37] J.-G. Park, M. D. Le, J. Jeong, and S. Lee, J. Phys.: Condens. Matter **26**, 433202 (2014).

[38] C. T. Nelson, P. Gao, J. R. Jokisaari, C. Heikes, C. Adamo, A. Melville, S.-H. Baek, C. M. Folkman, B. Winchester, Y. Gu, et al., Science **334**, 968 (2011).

[39] F. Gervais, *Infrared and Millimeter Waves* (Academic Press, 1983), vol. 8, chap. 7, p. 279.

[40] V. Železný, I. Fedorov, and J. Petzelt, Czech. J. Phys. **48**, 537 (1998).

[41] P. Hermet, M. Goffinet, J. Kreisel, and P. Ghosez, Phys. Rev. B **75**, 220102 (2007).

[42] R. H. Lyddane, R. G. Sachs, and E. Teller, Phys. Rev. **59**, 673 (1941).

[43] V. Goian, S. Kamba, N. Orloff, T. Birol, C. H. Lee, D. Nuzhnyy, J. C. Booth, M. Bernhagen, R. Uecker, and D. G. Schlom, Phys. Rev. B **90**, 174105 (2014).

[44] S. Kamba, V. Goian, D. Nuzhnyy, V. Bovtun, M. Kempa, J. Prokleška, M. Bernhagen, R. Uecker, and D. G. Schlom, Phase Transitions **86**, 206 (2013).

[45] C. M. Folkman, H. W. Jang, C. B. Eom, C. T. Nelson, X. Q. Pan, Y. L. Li, L. Q. Chen, A. Kumar, V. Gopalan, and S. K. Streiffer, Appl. Phys. Lett. **94**, 251911 (2009).

[46] D. Sando, A. Barthélémy, and M. Bibes, J. Phys.: Condens. Matter **26**, 473201 (2014).

[47] M. P. V. Stenberg and R. de Sousa, Phys. Rev. B **85**, 104412 (2012), ibid. **80**, 094419 (2009).

[48] D. Nuzhnyy, J. Petzelt, S. Kamba, P. Kužel, C. Kadlec, V. Bovtun, M. Kempa, J. Schubert, C. M. Brooks, and D. G. Schlom, Appl. Phys. Lett. **95**, 232902 (2009).

[49] A. Tagantsev, V. Sherman, K. Astafiev, J. Venkatesh, and N. Setter, J. Electroceramics **11**, 5 (2003).

[50] I. Kézsmárki, U. Nagel, S. Bordács, R. S. Fishman, J. H. Lee, H. T. Yi, S. Cheong, and T. Rõõm, ArXiv e-prints (2015), 1505.00033.

[51] Y. Takahashi, R. Shimano, H. Murakawa, and Y. Tokura, Nature Phys. **8**, 121 (2012).